FOI-R--1617--SE
April 2005
ISSN 1650-1942
Scientific report

Gunnar Wijk, Mats Hartmann, Andreas Tyrberg

A model for rigid projectile penetration and perforation of hard steel and metallic targets

Weapons and Protection
SE - 147 25 Tumba

SWEDISH DEFENCE RESEARCH AGENCY
Weapons and Protection
SE-147 25 Tumba

FOI-R--1617—SE
April 2005
ISSN 1650-1942
Scientific report

Gunnar Wijk, Mats Hartmann, Andreas Tyrberg

A model for rigid projectile penetration and perforation of hard steel and metallic targets

Issuing organization	Report number, ISRN	Report type
FOI – Swedish Defence Research Agency Weapons and Protection SE-147 25 Tumba	FOI-R--1617—SE	Scientific report
	Research area code 5. Strike and protection	
	Month year April 2005	**Project no.** E2007
	Customers code 5. Commissioned Research	
	Sub area code 51 Weapons and Protection	

Author/s (editor/s)	Project manager
Gunnar Wijk Mats Hartmann Andreas Tyrberg	Gunnar Wijk
	Approved by
	Sponsoring agency
	Refereed by Bo Janzon

Report title

A model for rigid projectile penetration and perforation of hard steel and metallic targets

Abstract (not more than 200 words)

A model for rigid projectile penetration and perforation of hard steel and metallic target plates is suggested. The intended application is in computer programs for assessment of effects and vulnerability for complex targets, such as tanks, fighter aircraft and naval ships.

The target material resistance to penetration is assumed to be constant, corresponding to lateral displacement of the material along the projectile trajectory, until the front end of the projectile is sufficiently close to the rear surface, whereupon the remaining volume of target material in front of the projectile is crushed and forms secondary fragments. At the penetration depth where this occurs the force required for crushing equals the force required for continued lateral displacement of the target material. The secondary fragments are ejected with the same velocity as the projectile.

Keywords

penetration perforation rigid projectile model vulnerability lethality assessment

Further bibliographic information	Language English
ISSN 1650-1942	**Pages** 13 p.
	Price acc. to pricelist

Utgivare	Rapportnummer, ISRN	Klassificering
Totalförsvarets Forskningsinstitut – FOI Vapen och skydd 147 25 Tumba	FOI-R--1617—SE	Vetenskaplig rapport
	Forskningsområde 5. Bekämpning och skydd	
	Månad, år April 2005	**Projektnummer** E2007
	Verksamhetsgren 5. Uppdragsfinansierad verksamhet	
	Delområde 51 VVS med styrda vapen	

Författare/redaktör	Projektledare
Gunnar Wijk Mats Hartmann Andreas Tyrberg	Gunnar Wijk
	Godkänd av
	Uppdragsgivare/kundbeteckning
	Granskad av Bo Janzon

Rapportens titel (i översättning)

En modell för stela projektilers penetration och perforation av hårda mål av stål och metaller

Sammanfattning (högst 200 ord)

En modell för stela projektilers penetration och perforation av målplåtar av hårda stål och metaller föreslås. Modellen är avsedd att tillämpas i datorprogram för värdering av verkan och sårbarhet för komplexa mål som stridsvagnar, stridsflygplan och krigsfartyg. Målmaterialets inträngningsmotstånd antas vara konstant och motsvaras av att materialet längs projektilens väg flyttas sidledes tills det att projektilens främre ända är tillräckligt nära den bortre målytan, varvid det återstående materialet framför projektilen krossas och bildar sekundärsplitter. Vid det inträngningsdjup där detta inträffar är den kraft som behövs för krossning lika med den kraft som skulle behövas för fortsatt sidledes förflyttning av materialet. Sekundärsplittren kastas ut med samma hastighet som projektilen.

Nyckelord

penetration perforation stel projektil modell verkansvärdering sårbarhetsvärdering

Övriga bibliografiska uppgifter	Språk Engelska
ISSN 1650-1942	**Antal sidor:** 13 s.
Distribution enligt missiv	**Pris: Enligt prislista**

Table of contents

Notation

d_P	projectile diameter	[m]
F	projectile retardation force	[N]
BHN	Brinell Hardness number (also HB)	
G_T	shear modulus of target material	[Pa]
h	target thickness	[m]
h^*	transition thickness between penetration and perforation	[m]
h_T	thickness of target material that forms secondary fragments	[m]
L_P	projectile length	[m]
m_P	projectile mass	[kg]
m_T	mass of secondary fragments from target rear surface	[kg]
P	projectile penetration depth	[m]
p_i, p_i', p_i''	cavity expansion pressure	[Pa]
R, R'	boundary radius between elastic and plastic deformation	[m]
R_c	Rockwell C hardness	
R_T	axial target resistance	[Pa]
u	projectile penetration velocity	[m/s]
v_P	projectile impact velocity	[m/s]
v_{exit}	projectile velocity after perforation	[m/s]
W_p	minimum target perforation energy	[J]
Y_P	uniaxial yield strength of projectile material	[Pa]
Y_T	uniaxial yield strength of target material	[Pa]
β	target penetration resistance parameter	
γ	projectile sharpness parameter	
ρ_P	projectile density	[kg/m^3]
ρ_T	target density	[kg/m^3]
θ	half apex angle for a ogive-nose projectile	[^{o}]
ν_T	elastic contraction factor (Poisson ratio) of target material	

Introduction

Many models have been suggested for projectile penetration and perforation, where the projectile either penetrates rigidly or eroding. The penetration resistance is often assumed to be the sum of a constant strength R_T and a hydrodynamic part, which is proportional to the product of the target density ρ_T and the square of the instantaneous penetration velocity u [1, 2]. For a rigid projectile with a certain nose shape penetration depth cannot depend on the projectile material's yield strength Y_P or density ρ_P since it is always "strong enough" when it penetrates rigidly, but only on the projectile mass m_P and diameter d_P.

Initially the penetration resistance should increase since it is easier to displace target material in front of the projectile when the impacted surface is close. When the front end of the projectile is deep inside the target then the resistance should be stabilised at some constant value and it should drop again when the front end is coming close to the rear target surface. It is obvious that the way, in which the penetration resistance drops when the front end of the projectile comes close to the rear target surface, must be intimately related to the production of secondary fragments from the target in connection with projectile perforation.

Most other models neglect increasing penetration resistance close to the front face of the target plate as well as decreasing penetration resistance close to the back face and generation of fragments from the back face. In the model presented here, which is focused on perforation of hard metallic targets, decreasing penetration resistance and generation of fragments is incorporated whereas increasing penetration resistance close to the front face is neglected. Targets of ductile material, for which there is a collar around the exit hole and also a plug in front of the projectile if it is blunt, are not covered by the model. The penetration resistance is described with one non-dimensional parameter, which is assumed to incorporate both nose resistance and friction along the projectile. The model is mainly a combination of two previously suggested models [3, 4].

In the present form the model is also restricted to impact normal to the target surface. The model gives an eventual residual projectile velocity and a nominal mass of fragments from the back face of the target. The stochastic nature of fragmentation is neglected, as well as the mass distribution and velocity distribution of the fragments. At sufficiently high impact velocities projectiles will be deformed and then the model not applicable.

Basic model assumptions: constant target resistance during penetration and constant hole diameter

The simplest model for projectile penetration corresponds to constant retardation force $F=\beta Y_T$, where β is a target penetration resistance parameter and Y_T is the yield strength of the target, for all penetration depths. Accordingly the projectile makes a hole with the diameter d_P to the final penetration depth P, which is proportional to the impact energy

$$P=\frac{2 m_P v_P^2}{\pi d_P^2 \beta Y_T} \qquad (1)$$

Here m_P is the mass of the projectile and v_P is the impact velocity. A representative value for the resistance coefficient that is used in the calculations below is

$$\beta=5. \tag{2}$$

This choice is considered in the appendix and based on [5, 6, 7, 8].

A model for penetration and perforation

During the penetration phase the target material in front of the projectile is eventually displaced, mainly laterally, via elastic-plastic deformation. During the perforation phase the material in front of the projectile is fragmented. The perforation phase starts when the front end of the projectile is at some distance h^* from the rear surface of the target. The minimum perforation energy W_P for a plate of hard metallic material with the thickness h is suggested to be given by [3, 4]

$$W_p = \frac{\pi}{8} d_P \, h \, (\pi \, h + \gamma \, d_P) \, Y_T \tag{3}$$

when $h < h^*$, whereas otherwise

$$W_p = \frac{\pi}{4} \left(h - h^*\right) d_P^2 \, \beta \, Y_T + \frac{\pi}{8} d_P \, h^* \left(\pi \, h^* + \gamma \, d_P\right) Y_T \tag{4}$$

.

Here γ is an empirically determined parameter describing target perforation resistance. Accordingly W_P is a continuous function of the thickness h, which is a physically necessary requirement. From the physical point of view it is reasonable to assume that $\partial W_p / \partial h$ also is a continuous function of h. Then Eqs. (3) and (4) yield

$$h^* = \frac{d_P}{2\pi} (2\beta - \gamma) \, . \tag{5}$$

If the target thickness h is smaller than h^* there is no initial penetration phase. Then the projectile simply fragments the material in front of it.

The parameter γ increases with the "bluntness" of the projectile. In particular the value is about unity for projectiles with conical impact ends with apex angle $2\theta=55^o$ as in [3], whereas it is about two for projectiles with spherical impact ends as in [4].

It should be emphasised that β describes the whole penetration resistance whereas γ in Eqs. (3) – (5) only describes part of the perforation resistance. Accordingly it is understandable that the latter is smaller than the former.

The mass m_T of fragments is estimated as

$$m_T \approx \frac{\pi}{4} d_P^2 \, h_T \, \rho_T \, , \tag{6}$$

where h_T is the smaller of h and h^*.

The model assumes that the energy required for the perforation phase is used to break the mass m_T into many fragments, whereupon these are accelerated by being pushed out of the target by the projectile.

The difference between the impact energy and the minimum perforation energy in either Eq. (3) or (4) is available to become exit kinetic energy of the projectile and the fragments. If there is perforation with all exit material having the same exit velocity v_{exit} and there is no energy loss, for instance due to friction between the fragments and either the projectile or the remaining target material during acceleration of the fragments, then the exit velocity is

$$v_{exit} = \sqrt{\frac{m_P v_P^2 - 2W_P}{m_P + m_T}} \,. \tag{7}$$

When the target is so thick that perforation does not occur, then the penetration depth P is given by Eq. (1). If the calculated penetration depth is found in the interval $h - h^* < P < h$, then production of fragments starts but is halted when the projectile stops.

Comparison with experimental results

The suggested model is compared with published experimental results as shown in Figure 1 - Figure 8. All data used in the calculations are presented in Table 1.

Table 1: Projectile data used for model comparison with published results

	Brooks 1973 [9, 10]	Piekutowski et al 1999 [11]	5.56 APHC in steel HB 300 [12]	5.56 APHC in steel HB 500 [12]	7.62 APHC in steel HB 300 [13]	7.62 APHC in steel HB 500 [13]	Forrestal, Rosenberg, Luk and Bless 1987 [14,10]	Rosenberg and Forrestal 1988 [15,10]
	Figure 1	Figure 2	Figure 3	Figure 4	Figure 5	Figure 6	Figure 7	Figure 8
Projectile	tungsten carbide	steel R_c 38	tungsten carbide	tungsten carbide	tungsten carbide	tungsten carbide	steel	steel
m_P , g	37.4	20.4	2.0	2.0	6.0	6.0	78.0	~25
d_P , mm	10.16	7.11	4.0	4.0	5.6	5.6	9.53	7.10
γ	-	-	1	1	1	1	1	1
Target	steel	aluminium	steel	steel	steel	steel	aluminium	aluminium
Y_T , GPa	1.00	0.276	1.00	1.67	1.00	1.67	0.30	0.30
ρ_T , kg/m^3	7850	2710	7850	7850	7850	7850	2710	2710
h , mm	thick	thick	varies	varies	varies	varies	25.4	25.4

Penetration depth results

Figure 1 and Figure 2 show penetration depth P in steel and aluminium as functions of the projectile impact velocity v_P.

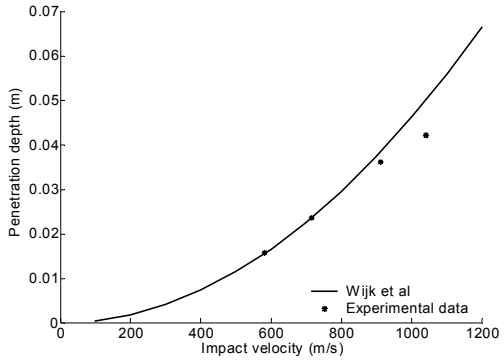

Figure 1: Brooks 1973

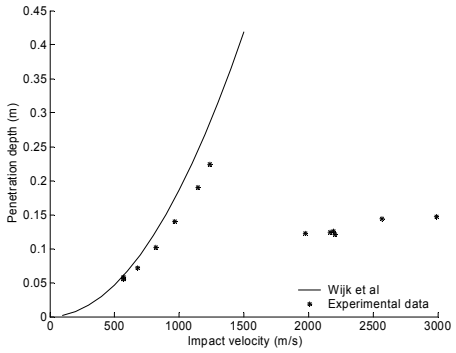

Figure 2: Piekutowski et al 1999, R_C 38

Limit velocity results

Figure 3 - Figure 6 show the maximum perforation thickness as function of the impact velocity for APHC projectiles for two qualities of steel armour. The points in the diagrams are not actual experimental data but are taken with the interval 100 m/s from the graphs in the [12, 13]. The transition thicknesses, according to Eq. (5), for the two projectiles are 6 and 8 mm, respectively. Thus the results cover both thin and thick targets in the sense of Eqs. (2) – (4).

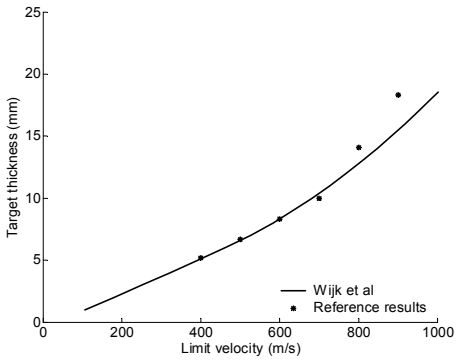

Figure 3: 5.56 APHC in steel HB 300

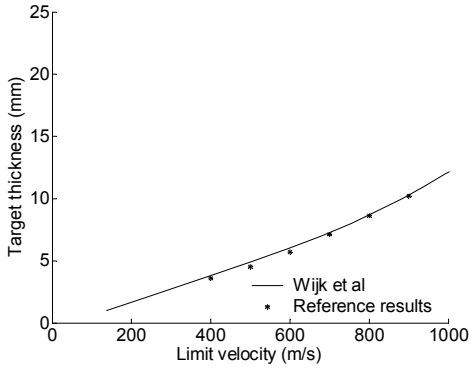

Figure 4: 5.56 APHC in steel HB 500

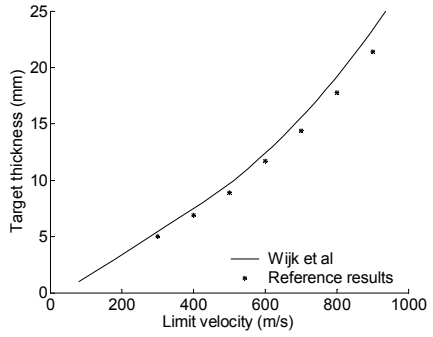

Figure 5: 7.62 APHC in steel HB 300

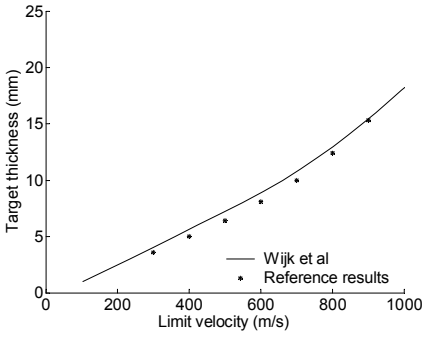

Figure 6: 7.62 APHC in steel HB 500

Residual velocity results

Figure 7 and Figure 8 show the residual projectile velocity after perforation of aluminium target plates. The connection thicknesses, according to Eq. (5), for the two cases are $h^* \approx 13$ and 10 mm, respectively. Eq. (6) yields the masses of fragments to be 1.3 and 1.1 g, which are negligible compared to the projectile masses. Thus they do not influence the total kinetic energy after perforation significantly.

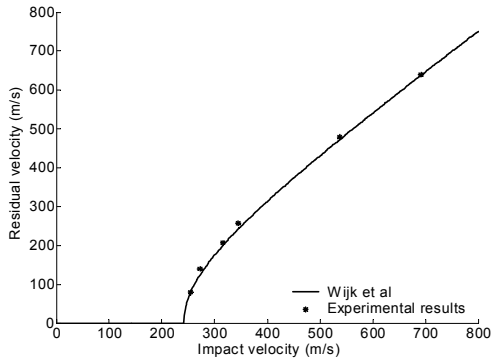

Figure 7: Forrestal, Rosenberg, Luk and Bless (1986)

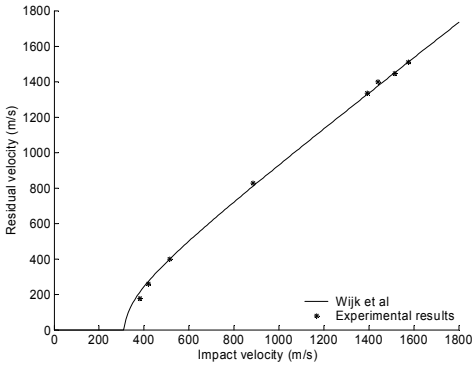

Figure 8: Rosenberg and Forrestal (1988)

Discussion

The model seems to overestimate the projectile penetration capacity when it is used to predict penetration depths in semi-infinite targets. This can be seen quite clearly in Figure 2 and the same tendency can also be found in Figure 1. One reason is probably that the projectile nose shape has some influence on the penetration performance. Another reason may be that penetration resistance at the nose and friction along the projectile should be accounted for separately. Despite this the model is presented with the proposed constant $\beta=5$ in Eq. (2) since the results are in good enough agreement when the impact velocity is above the ballistic limit.

Calculations of limit velocity yield reasonable agreement with the reference results. In the cases of 7.62 mm APHC, Figure 5 and Figure 6, the model slightly overestimates the maximum perforation thickness. In this case the nose shape is accounted for, at least in principle, via the nose shape parameter γ in Eqs. (3) - (5).

The model predictions of the residual velocity are in good agreement with the presented experimental results, Figure 7 and Figure 8. This is an encouraging result for the intended use of the model, since the residual velocity is one of the most important quantities in assessment of vulnerability and survivability.

The yield strengths in GPa for the target materials are in some cases estimated by dividing the BHN with 300. This is of course a coarse way to determine such a critical input value, especially when results from different sources are compared.

Conclusion

The model suggested above assumes that the minimum perforation energy is independent of the impact velocity and that it increases with the target thickness. Consequently a certain combination of projectile density, shape and diameter and target strength and thickness corresponds to a minimum impact velocity for perforation. For greater impact velocities the projectile will emerge with an exit velocity together with a bundle of fragments.

The general agreement between the model and experimental results is reasonably good. When preceding penetration depth is about equal to subsequent perforation thickness, then the penetration coefficient will necessarily be somewhat smaller than for deep penetration without subsequent perforation. Nevertheless the penetration coefficient $\beta=5$ yields acceptable results for cases of primary interest for the intended applications, namely in assessments of effects and vulnerability for complex targets.

Friction and initial penetration resistance is neglected in the model. These are two phenomena that should be incorporated in a development of the model. The model is restricted to hard metallic targets and impact along the normal direction of the target face and only gives a nominal mass of fragments. Consequently it is necessary to continue to develop the model before it really can be used for assessment of effects and vulnerability.

References

1 J. A. Zukas
High Velocity Impact Dynamics
John Wiley & Sons, New York, 1990

2 M. A. Meyers
Dynamic Behaviour of Materials
John Wiley & Sons, New York, 1994.

3 A. G. Wijk
Sharp-Nosed Projectile Perforation of Target Plates
FOA-R--99-01106-310--SE

4 A. G. Wijk
Blunt-Nosed Projectile Perforation of Target Plates
FOA-R--99-01181-310--SE

5 A. Gunnar Wijk
High-velocity projectile penetration into thick armour targets
International Journal of Impact Engineering 22 (1999) 45-54

6 A. L. Yarin, M. B. Rubin and I. V. Roisman
Penetration of a rigid projectile into an elastic-plastic target of finite thickness
Int. J. Impact Engng. Vol. 16, No. 5/6, pp. 801-831, 1995

7 G. Yossifon, M. B. Rubin, A. L. Yarin
Penetration of a rigid projectile into a finite thickness elastic-plastic target - comparison between theory and numerical simulations
International Journal of Impact Engineering 25 (2001) 256-290

8 Michael J. Forrestal, Andrew J. Piekutowski
Penetration experiments with 6061-T6511 aluminium targets and spherical-nose steel projectiles at striking velocities between 0.5 and 3.0 km/s
International Journal of Impact Engineering 24 (2000) 57-67

9 P. N. Brooks
On the prediction of crater profiles produced in ductile targets by the impact of rigid penetrators at ballistic velocities
Defence Research Establishment Valcartier, DREV R-686/73
10 Charles E. Anderson, Jr., Bruce L. Morris, David L. Littlefield
A Penetration mechanics data base
Southwest Research Institute, SwRI report 3593/001, 1992
11 Andrew J. Piekutowski, Michael J. Forrestal, Kevin L. Poormon and Thomas L. Warren
Penetration of 6061-T6511 Aluminium targets by ogive-nose steel projectiles with striking velocities between 0.5 and 3.0 km/s
International Journal of Impact Engineering 23 (1999) 723-734
12 Bofors Carl Gustaf, Celcius Group
In Position of Power: CG 5.56 mm AP
Eskilstuna, Sweden, 1997
13 Bofors Carl Gustaf, Celcius Group
In Position of Power: CG 7.62 mm AP
Eskilstuna, Sweden, 1997]
14 M. J. Forrestal, Z. Rosenberg, V. K. Luk, S. J. Bless
Perforation of Aluminum Plates With Conical-Nosed Rods
Journal of Applied Mechanics, vol. 54, pp. 230-232, March 1987
15 Z. Rosenberg and M. J. Forrestal
Perforation of Aluminum Plates With Conical-Nosed Rods - Additional Data and Discussion
Journal of Applied Mechanics, vol. 55, pp. 236-238, March 1988

Appendix: Discussion of constant penetration resistance

Constant penetration resistance, represented by $\beta=5$ in Eq. (2), was first suggested with reference to quasi-static arguments [5]. A combination of cylindrical and spherical quasi-static cavity expansion is used to derive the approximate relation

$$\beta=\frac{R_T}{Y_T}\approx 5. \tag{A1}$$

for deep hole penetration resistance. Thereby it is assumed that the material that is plastically deformed is incompressible. Below considerably better theoretical results than those in [5], namely for compressible plastic deformation from [8], are used for this purpose. Cylindrical elastic-plastic expansion from zero hole diameter to the projectile diameter corresponds to the plastic deformation to the radius R

$$R=\frac{d_P}{2}\sqrt{\frac{4(1+\nu_T)G_T}{(5-4\nu_T)Y_T}}. \tag{A2}$$

Here G_T and ν_T are the shear modulus and the Poisson ratio for the target material. The corresponding pressure in the hole is given by the (statically determinate) state of stress in the plastically deformed region

$$p_i=Y_T\left\{\log\left(\frac{2R}{d_P}\right)+\frac{1}{2}\right\}. \tag{A3}$$

The corresponding results for spherical elastic-plastic cavity expansion are

$$R'=\frac{d_P}{2}\sqrt[3]{\frac{2(1+\nu_T)G_T}{3(1-\nu_T)Y_T}}. \tag{A4}$$

and

$$p_i'=2Y_T\left\{\log\left(\frac{2R'}{d_P}\right)+\frac{1}{3}\right\}. \tag{A5}$$

The spherical hole pressure is somewhat greater and the plastic radius is somewhat smaller than the corresponding quantities for a cylindrical hole. The real plastic boundary around the end of a deep cylindrical hole should be rather well approximated by R' straight ahead of the hole and by R along the hole (except in the vicinity to the hole entrance). The real plastic boundary should be a smooth surface around the end of the hole, and the radius should be close to R in the plane that contains the bottom of the hole. A simple smooth surface is obtained if the plastic radius in front of the hole bottom is R instead of R'. According to Eqs. (A2) and (A5) the pressure on the hole bottom is then given by

$$p_i'' = 2\,Y_T \left\{ \log\left(\frac{2R}{d_P} \right) + \frac{1}{3} \right\}. \qquad \text{(A6)}$$

For steel with G_T=*80* GPa, ν_T=*0.3* and Y_T=*1.0* GPa Eqs. (A2) (A3) and (A6) yield $p_i' \approx 3.7\,Y_T$ and $p_i'' \approx 5.3\,Y_T$. Since the real plastic radius straight ahead of the projectile should be somewhat smaller than R but significantly greater than R' it follows that the real hole production pressure should be somewhat smaller than p_i'' and significantly greater than p_i'. Accordingly the estimate in Eq. (A1) is obtained.

Recently considerably more advanced numerical calculations [7], which account for the dynamic situation in a realistic manner, yield essentially the result that the penetration resistance for a rigid round-nosed projectile is about five times the yield strength when the penetration depth is several times greater than projectile diameter. A figure in [7] shows the penetration velocity u and the retardation force F acting on the rigid projectile as functions of the penetration depth P for four different models, two analytical and two numerical (Autodyn). The differences between the four results are marginal, so that the "average" is represented by the graphs in Figure 9. The retardation force is initially zero and increases with the penetration depth. With the actual values in [7], the limiting value for the penetration force in Figure 9 corresponds to $\beta \approx 4.5$.

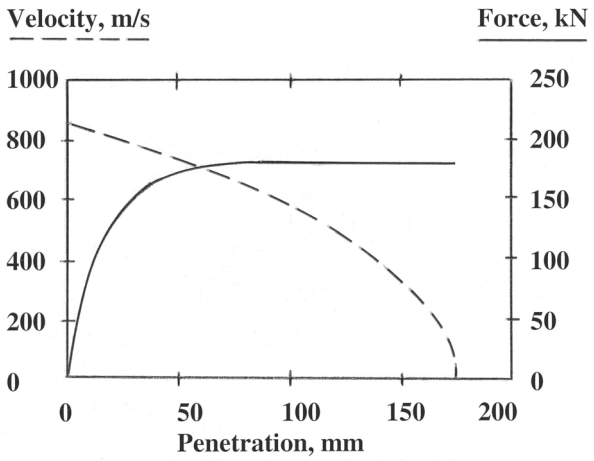

Figure 9: "Average" results from [7, Figure 6] for the instantaneous velocity and the corresponding retardation force as functions of rigid projectile penetration.

It should be pointed out that there is separation between the projectile and the laterally displaced target material about $2d_P$ behind the front end of the projectile (the projectile shape is an ovoid of Rankine). The total length of the projectile is L_P=$5d_P$. Accordingly there is certainly no friction along the last part of the projectile. However, since a friction coefficient is specified there is no friction force in the model in [7]. If this model underestimates the real elastic reaction of the target material behind the front part of the projectile and there is non-vanishing friction, then experimental results should yield a value of the "apparent" nose penetration coefficient β that is greater than the value 4.5 from Figure 9.